THE JOURNAL OF BIOLOGICAL CHEMISTRY VOL. 289, NO. 36, pp. 25054–25066, September 5, 2014
© 2014 by The American Society for Biochemistry and Molecular Biology, Inc. Published in the U.S.A.

Amino Acid Derivatives as Bitter Taste Receptor (T2R) Blockers*

Received for publication, April 30, 2014, and in revised form, July 15, 2014 Published, JBC Papers in Press, July 24, 2014, DOI 10.1074/jbc.M114.576975

Sai P. Pydi[‡§1], Tyler Sobotkiewicz[‡1,2], Rohini Billakanti[‡§2], Rajinder P. Bhullar[‡], Michele C. Loewen[¶], and Prashen Chelikani[‡§3]

From the [‡]Department of Oral Biology, University of Manitoba, Winnipeg, Manitoba R3E 0W4, the [§]Manitoba Institute of Child Health, Winnipeg, Manitoba R3E 0W4, and the [¶]National Research Council of Canada, Saskatoon, Saskatchewan S7N 0W9, Canada

Background: T2Rs are activated by hundreds of bitter compounds; however, only five blockers are known.
Results: T2R4 residues involved in binding to agonist quinine and two novel bitter blockers GABA and BCML were identified.
Conclusion: Bitter blockers and agonists share the same orthosteric site in T2R4.
Significance: Bitter blockers identified in this study have tremendous physiological and nutraceutical importance.

In humans, the 25 bitter taste receptors (T2Rs) are activated by hundreds of structurally diverse bitter compounds. However, only five antagonists or bitter blockers are known. In this study, using molecular modeling guided site-directed mutagenesis, we elucidated the ligand-binding pocket of T2R4. We found seven amino acids located in the extracellular side of transmembrane 3 (TM3), TM4, extracellular loop 2 (ECL2), and ECL3 to be involved in T2R4 binding to its agonist quinine. ECL2 residues Asn-173 and Thr-174 are essential for quinine binding. Guided by a molecular model of T2R4, a number of amino acid derivatives were screened for their ability to bind to T2R4. These predictions were tested by calcium imaging assays that led to identification of γ-aminobutryic acid (GABA) and *Nα*,*Nα*-bis(carboxymethyl)-L-lysine (BCML) as competitive inhibitors of quinine-activated T2R4 with an IC_{50} of 3.2 ± 0.3 μM and 59 ± 18 nM, respectively. Interestingly, pharmacological characterization using a constitutively active mutant of T2R4 reveals that GABA acts as an antagonist, whereas BCML acts as an inverse agonist on T2R4. Site-directed mutagenesis confirms that the two novel bitter blockers share the same orthosteric site as the agonist quinine. The signature residues Ala-90 and Lys-270 play important roles in interacting with BCML and GABA, respectively. This is the first report to characterize a T2R endogenous antagonist and an inverse agonist. The novel bitter blockers will facilitate physiological studies focused on understanding the roles of T2Rs in extraoral tissues.

Human bitter taste perception is mediated by 25 bitter taste receptors (T2Rs) (1, 2). T2Rs are activated by a wide range of compounds, which include peptides, alkaloids, terpenoids, and amines. In addition to the oral cavity, T2Rs are expressed in extraoral tissues, including nasal epithelium (3), brain (4, 5), large intestine (6, 7), testis, and human airways (8, 9). T2Rs form a distinct subfamily within the G protein-coupled receptor (GPCR)[4] superfamily. T2Rs are one of the least studied and understood GPCR subfamilies. Structure-function studies to understand ligand binding have been carried out on 9 of the 25 T2Rs, including T2R1 (10), T2R10 (11), T2R14 (12), T2R16 (13), T2R30 (14), T2R38, T2R43, T2R44 (T2R31), and T2R46 (15). In T2Rs, the extracellular residues on transmembrane (TM) helices TM3, TM6, and TM7 are predominantly involved in ligand binding. Better understanding of the T2R-ligand interactions will provide novel tools for modulating receptor function in various physiological and pathophysiological conditions.

T2Rs are activated by structurally diverse natural and synthetic bitter compounds (16). Many common pharmaceutical compounds are bitter in taste, and these are effective ligands for T2Rs. For example, antimalarial drugs like quinine and chloroquine and antibiotics like erythromycin and ofloxacin can activate T2Rs. In addition, T2Rs expressed in extraoral tissues may mediate the off-target action of these drugs. Therefore, a better understanding of T2Rs and identification of their blockers (antagonists and inverse agonists) will help in eliminating these off-target drug effects. The development of bitter blockers will help in masking the bitter taste of drugs. Children's medications are predominantly liquid formulations, and it is extremely difficult to mask the flavors of these bitter medicines. A better understanding of the ligand-binding pocket of T2Rs and development of bitter blockers may yield new ways of overcoming these unpleasant flavors and increase compliance of medications and palatability of certain bitter-tasting health foods. Thus far, only five bitter blockers have been published (17–20). These block nine T2Rs with different efficacies, with

* This work was supported in part by Discovery Grant RGPIN 356285 from Natural Sciences and Engineering Research Council of Canada and operating grants from Manitoba Medical Service Foundation and Manitoba Health Research Council (to P. C.).
[1] Supported by studentships from Manitoba Health Research Council/Manitoba Institute of Child Health.
[2] These authors contributed equally to this work.
[3] Supported by a Manitoba Medical Service Foundation Allen Rouse Career Award. To whom correspondence should be addressed: D319, Dept. of Oral Biology, University of Manitoba, Winnipeg, Manitoba R3E 0W4, Canada. Tel.: 204-789-3539; Fax: 204-789-3913; E-mail: Prashen.Chelikani@umanitoba.ca.

[4] The abbreviations used are: GPCR, G protein-coupled receptor; BCML, *Nα*,*Nα*-bis(carboxymethyl)-L-lysine; TM, transmembrane; OA, L-ornithyl-β-alanine; CAM, constitutively active mutant; RFU, relative fluorescence unit; IP_3, inositol triphosphate; GIV3727, 4-(2,2,3-trimethylcyclopentyl) butanoic acid; AGE, advanced glycation end.

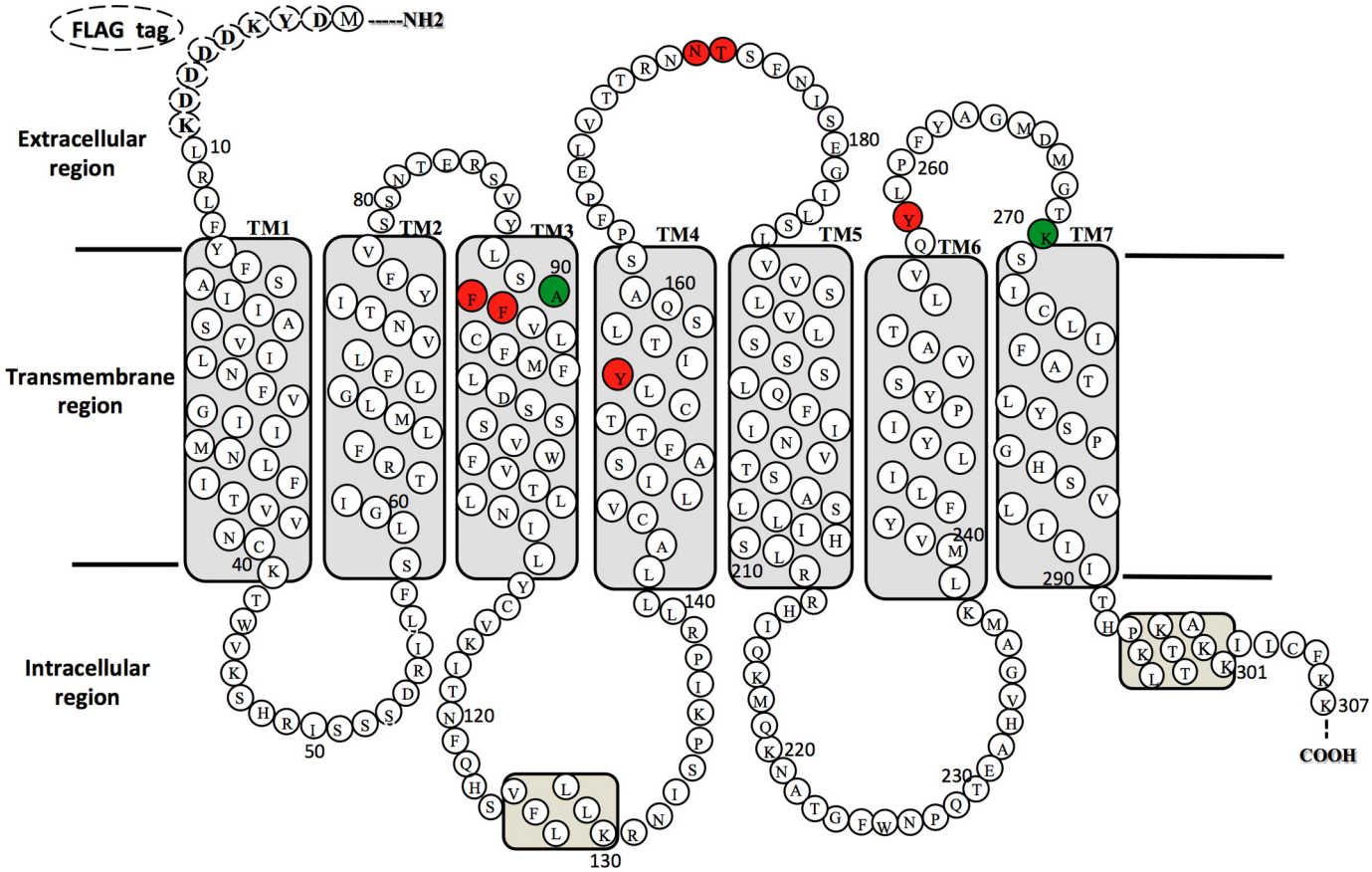

FIGURE 1. **Schematic representation of the amino acid sequence of T2R4 with ligand-binding pocket residues highlighted.** The amino acid sequence of T2R4 consists of 307 residues, including the FLAG tag sequence in the short N terminus. T2R4 consists of seven TM helices (TM1–7), three extracellular loops, and three intracellular loops and a short C terminus. T2R4 residues involved in ligand binding and subjected to site-directed mutagenesis are predominantly located in the extracellular side and are highlighted in different *colors*. Amino acids important for quinine binding are represented in *red,* and residues important for binding to bitter blockers are colored in *green*.

the best known blocker 4-(2,2,3-trimethylcyclopentyl) butanoic acid (GIV3727) displaying a half-maximal inhibitory concentration (IC_{50}) of 6 μM (17).

Low molecular weight compounds, which include amino acid derivatives and peptides, are known to mask bitter taste. However, the mechanism(s) of masking bitter taste, whether the compounds act at the receptor level or on the intracellular components of the taste signaling cascade, was not elucidated. Previous studies suggest L-ornithyl-β-alanine (OA) masks the bitter taste of potassium salt, and γ-aminobutyric acid (GABA) masks the bitter taste of quinine, caffeine, coca, and chocolate (21). We hypothesized that these amino acid derivatives may act at the receptor level as T2R blockers. To test this hypothesis, T2R4 was used as a model (Fig. 1). Quinine a natural alkaloid with a quinoline ring and a bicyclic quinuclidine is one of the most bitter-tasting compounds and was previously shown to activate T2R4, although its binding site was not determined (16, 22, 23). Indeed, there is no structure-function information on the ligand-binding pocket of T2R4. In this study, amino acids involved in T2R4 binding to quinine were elucidated using a combination of approaches consisting of molecular modeling, site-directed mutagenesis, and functional characterization by IP_3 and calcium imaging assays.

The results from this work suggest that different ligands bind within the orthosteric site in T2R4. Two novel bitter blockers of important nutraceutical and physiological importance are also characterized. We report that GABA, an inhibitory neurotransmitter, acts as a T2R4 antagonist. This makes GABA the first known endogenous T2R antagonist. In addition, BCML is the first T2R antagonist to show inverse agonist property.

EXPERIMENTAL PROCEDURES

Materials—DMEM/F-12, penicillin, streptomycin, L-glutamine, trypsin/EDTA, calcium-sensitive dye Fluo-4 NW, and Lipofectamine 2000 were purchased from Invitrogen. GABA, BCML, and fetal bovine serum (FBS) were purchased from Sigma. Common chemicals and bitter compounds were purchased either from Fisher or Sigma. All chemicals were of analytical grade and used without further purification. The Gα16/44 chimera was a gift from Dr. Takashi Ueda, Nagoya City University, Japan.

Molecular Biology and Cell Culture—The WT-TAS2R4 with the octapeptide FLAG tag at the N terminus was described previously (23, 24). WT-TAS2R4 and mutant genes were codon-optimized for expression in mammalian cells, to minimize variations in expression. The mutants were synthesized commercially (Genscript USA Inc.). All the constructs were in pcDNA 3.1 and expressed in HEK293T cells according to our previously published protocols (23, 24). In all functional and cell surface expression studies, the amount of plasmid DNA

used in each transfection was kept constant at 3 μg per 3×10^6 cells, unless otherwise specified. Following transient transfection, viable cells as determined on a Bio-Rad TC10 automated cell counter were used for different assays.

Flow Cytometry—Studies of cell surface expression of T2R4 and the mutants were carried out using flow cytometry with anti-FLAG antibody (25). HEK293T cells were transfected with pcDNA3.1 or pcDNA3.1 containing the WT-TAS2R4 or mutant genes using Lipofectamine 2000. After 24 h of transfection, 1×10^5 viable cells were taken into a tube and washed twice with 1× PBS containing 0.5% BSA (FACS buffer), and cells were collected by centrifugation for 4 min at 1500 rpm. The cells were fixed using 2% paraformaldehyde by incubating for 10 min. Cells were then incubated for 1 h on ice with monoclonal FLAG antibody diluted (1:200) in PBS. After three washings with FACS buffer, cells were incubated with secondary antibody Alexa-488 diluted (1:500) in PBS for 1 h on ice. Cells were again washed three times with FACS buffer and resuspended in 500 μl of FACS buffer, and the fluorescence signals of at least 10^4 cells/tube were measured using single color analysis by FACS Canto analyzer. The results are analyzed using FACS Diva and FlowJo software and represented in mean fluorescence intensities. All data shown are mean values ± S.E. for n = 3–5 determinations.

Ca^{2+} Mobilization—Functional characterization of the WT-T2R4 and mutants was carried out by measuring the intracellular Ca^{2+} release from endoplasmic reticulum using the Fluo-4 NW calcium assay kit. HEK293T cells were transfected with pcDNA3.1 or pcDNA3.1 containing the WT-TAS2R4 or mutant genes. Cells transfected with pcDNA3.1 vector were used as a negative control (mock-transfected cells). After 6–8 h of transfection, a viable cell count was taken, and 1×10^5 cells/well were plated in 96-well clear bottom black-walled plates. Cells were incubated at 37 °C in a CO_2 incubator for 16 h. Then the culture medium was removed, and cells were incubated with Fluo-4 NW dye for 40 min at 37 °C and 40 min at room temperature. Fluo-4 NW dye was prepared by dissolving lyophilized dye in 10 ml of assay buffer (1× Hanks' balanced salt solution, 20 mM HEPES), and probenecid (2.5 mM) was added to block the leakage of dye from cytosol. The above components (Fluo-4 NW dye, assay buffer, and probenecid) are from the Fluo-4 NW calcium assay kit and used as recommended by the manufacturer. Calcium was measured in terms of relative fluorescence units (RFUs) using a Flexstation-3 microplate reader. The basal intracellular calcium levels were measured for the first 20 s, and then the appropriate concentration of ligands was added by the built-in 8-channel pipette of Flexstation-3, and calcium readout continued for another 120 s. To get the absolute RFUs, the basal RFU before adding the ligand (minimum (Min)) was deducted from the peak RFU (maximum (Max)) obtained after stimulating with the ligand (absolute RFUs = Max − Min). Next, the signals from the mock-transfected cells were deducted from the observed signal to give ΔRFUs (ΔRFUs = WT or mutant absolute RFUs − mock-transfected absolute RFUs).

In functional characterization of WT-T2R4 and mutants, agonist (quinine) concentration used was from 4 to 0.062 mM (half-way serial dilution). For elucidating the IC_{50} value of potential bitter blockers, HEK293T cells expressing T2R4 or mutants were treated with the potential blockers (concentrations ranging from 1 mM to 0.01 nM) in the presence of 1 mM quinine (its $\sim EC_{50}$ value). The results were analyzed using PRISM software version 4.03 (GraphPad Software, San Diego).

IP_3 Assay—Activated T2R couples to G-protein, which activates phospholipase C-β2. The phospholipase C-β2 cleaves phosphatidylinositol 4,5-bisphosphate into diacylglycerol and IP_3. Thus, IP_3 was measured to characterize the signaling efficacy of WT and mutant T2Rs. This is a competition-binding assay, where intracellular IP_3 and fluorescently labeled IP_3 compete to bind with the IP_3-binding protein. An IP_3 standard graph was generated using known concentrations of IP_3 (20 pM to 20 μM), and the fluorescence was measured according to the instructions provided by the manufacturer (HitHunter IP_3 Fluorescence Polarization assay kit, DiscoveRx). This standard graph was used to measure the agonist-dependent and agonist-independent IP_3 produced by cells. 10^5 cells/well expressing WT-T2R4 or the mutants were plated in black-walled plates and treated with a single concentration of ligand or with buffer. The amount of IP_3 produced was reported in terms of picomoles.

Statistical Analysis—PRISM statistical analysis software version 4.03 was used to analyze the bar plots and to identify EC_{50} and IC_{50} values of dose-response curves. To analyze the significance among different columns in bar plots, one-way analysis of variance followed by Tukey's multiple comparison post hoc test was done ($p < 0.05$ considered as significant).

Molecular Modeling—The T2R4 amino acid sequence was obtained from NCBI. Sequence without the FLAG tag was submitted to the I-TASSER server for model building. The inactive T2R4 model was built using the crystal structure of rhodopsin (Protein Data Bank code 1U19), and an active T2R4 model was built using transducin C-terminal bound opsin crystal structure (Protein Data Bank code 3DQB). Transmembrane regions of T2R4 were predicted by TMpred and HMMTOP servers. The loop regions of the receptor were modeled using the Mod Loop server. Amino acid side chains of the receptor were refined using the SCWRL4 program. Staged minimization was performed using the steepest descent and conjugate gradient algorithms. Molecular dynamics simulations were carried out with a time step of 2 fs. Quality of the model was checked using Procheck. A90F and K270A mutant models were generated using PyMOL and energy-minimized as described above. These receptor models were used for ligand docking.

Ligand Docking and Scoring—All the ligand structures were obtained from PubChem and the derivatives from the parent structures, using the SYBYL-X 1.3 suite (CERTARA^{TM}). These molecules were energy-minimized for further use. Docking of T2R4 with the ligands was carried out using Surflex-Dock of the SYBYL-X 1.3 suite. Surflex-Dock uses an empirical scoring function to dock ligand into a protein-binding site. The ligand was held rigid while keeping the receptor flexible during the refinement. This was done to maintain a specific conformation of the ligand. The search grid extended 6 Å beyond protein dimensions. The maximum number of conformations (active site) per fragment submitted to the docking procedure was set to 20. The geometry of the ligands was optimized before and

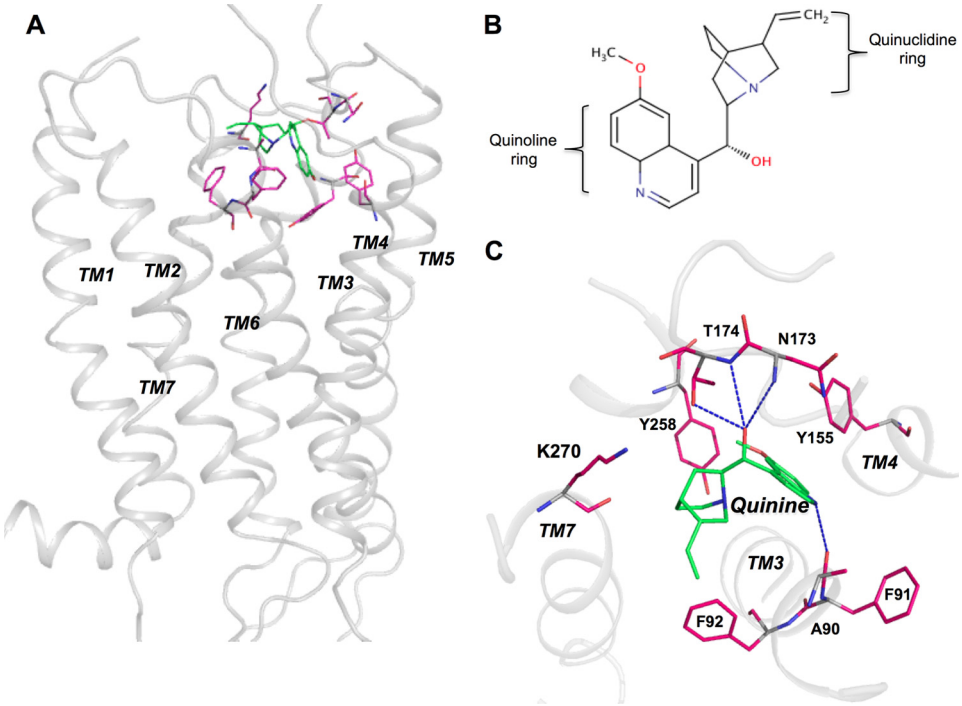

FIGURE 2. **Molecular model of quinine bound to T2R4.** *A,* three-dimensional model of T2R4-quinine complex. A homology model of T2R4 was built and quinine docked using Surflex-Dock program of SYBYL-X 1.3 suite as described under "Experimental Procedures." TM1–7 are colored in *gray* and quinine in *green*, and the amino acids within 4 Å of quinine are shown in *pink*. *B,* chemical structure of quinine (PubChem CID 8549). Quinine, a natural alkaloid, consists of an aromatic quinoline ring and a bicyclic quinuclidine. *C,* quinine-binding pocket in T2R4. Residues Ala-90, Phe-91, Phe-92, Tyr-155, Asn-173, Thr-174, Tyr-258, and Lys-270 that are within the 4 Å region are shown. *Blue dotted lines* denote the hydrogen bonding between quinine and T2R4 amino acids.

after docking using the BFGS quasi-Newton method and internal dreiding force field. A maximum of 10 poses was saved for each ligand. The final step in docking is the scoring of the refined docked poses. The binding affinities of protein-ligand complexes were obtained as the total Surflex-Dock score expressed as $-\log (K_d)$.

RESULTS

Prediction of Quinine-binding Site in T2R4—Quinine was docked to the T2R4 model using the Surflex-Dock of SYBYL-X 1.3 suite as described under "Experimental Procedures." The ligand-binding pocket was located in the extracellular side of T2R4 (Fig. 2*A*). Quinine is a fusion product of an aromatic quinoline ring and a bicyclic quinuclidine (Fig. 2*B*). The quinoline ring has two functional groups, one methoxy and an amine, whereas the bicyclic quinuclidine has an amine. A hydroxyl group is present at the junction of the quinoline and quinuclidine rings. Based on molecular modeling, the different functional groups of quinine are primarily involved in H-bonding with the T2R4 residues. These functional groups were involved in interactions with the backbone or side chains of T2R4 amino acids Ala-90, Phe-91, Tyr-155, Tyr-258, and Lys-270 (Fig. 2*C*).

Site-directed Mutagenesis and Characterization of T2R4 Residues Involved in Quinine Binding—To elucidate the amino acids involved in quinine binding in T2R4, a molecular model guided mutagenesis approach was followed. Twelve site-directed mutants were engineered at eight positions in T2R4, and two types of mutations were made. First, mutations were made to a smaller amino acid such as alanine or glycine (if the amino acid being mutated is an alanine), with the expectation that this substitution will have a minimal effect on receptor folding and ligand binding. Second, mutations were made with either a nonconserved substitution such as alanine to phenylalanine or with conserved substitution such as lysine to arginine. The constructs containing the mutants were transiently expressed in HEK293T cells. A90G, A90F, F91A, and F92A mutants were located in TM3; Y115A was in TM4; N173A, N173Q, T174A, and T174S were in ECL2; and Y258A, K270A, and K270R were in ECL3 (Fig. 1). The mutants were characterized for their function and expression.

Functional analysis of WT-T2R4 and mutant receptors was determined by measuring changes in intracellular calcium mobilization of HEK293T cells transiently expressing these receptors after application of different concentrations of quinine. The mutants displayed varied levels of signaling (Fig. 3). Mutation of Ala-90 showed interesting results (Fig. 3 *A, panel I*). For the A90G mutant, where alanine was replaced with a simple amino acid glycine, which has no functional group, quinine treatment resulted in no detectable calcium mobilization compared with WT-T2R4. However, replacement of the alanine with a bulky aromatic phenylalanine, as in the A90F mutant, resulted in a hyperactive mutant with an upward and right shift of the dose-response curve with an EC_{50} value of 1241 ± 190 μM compared with 627 ± 80 μM for WT-T2R4 (Fig. 3*A, panel I*). The F91A mutant was activated by quinine and caused a significant increase in intracellular calcium mobilization but not in a quinine concentration-dependent manner (Fig. 3*A, panel II*). In contrast, F92A showed a response similar to WT-T2R4, with an EC_{50} value of 810 ± 150 μM. Analysis of

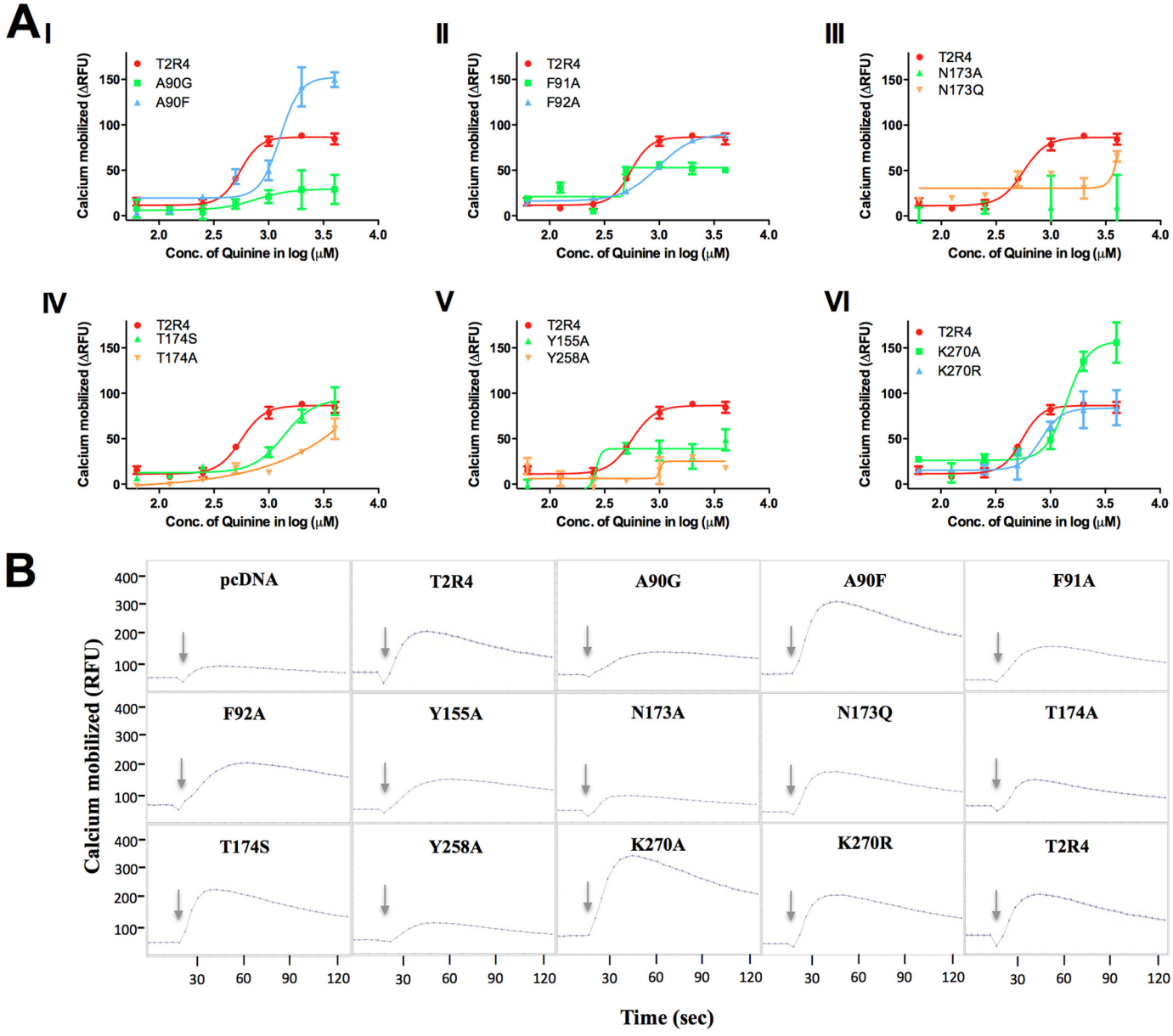
A
I
T2R4
A90G
A90F
II
T2R4
F91A
F92A
III
T2R4
N173A
N173Q
IV
T2R4
T174S
T174A
V
T2R4
Y155A
Y258A
VI
T2R4
K270A
K270R
Calcium mobilized (ΔRFU)
Conc. of Quinine in log (μM)
B
pcDNA
T2R4
A90G
A90F
F91A
F92A
Y155A
N173A
N173Q
T174A
T174S
Y258A
K270A
K270R
T2R4
Calcium mobilized (RFU)
Time (sec)
C
Cell surface expression normalized to wild type receptor expression
T2R4
A90G
A90F
F91A
F92A
Y155A
N173A
N173Q
T174A
T174S
Y258A
K270A
K270R

the TM4 and ECL2 mutants Y155A, N173A, N173Q, T174A, and T174S showed that, except for T174S, none of the other mutants displayed a quinine-dependent increase in calcium mobilization (Fig. 3*A*, *panels III–V*). The T174S mutant showed a right shift in the dose-response curve and close to a 2-fold increase in the EC_{50} value of 1612 ± 395 μM compared with 627 ± 80 μM for WT-T2R4. The two residues, Tyr-258 and Lys-270, present in ECL3, are predicted to play a role in quinine binding. The Y258A mutant displayed no quinine-dependent calcium mobilization. Interestingly, the K270A mutant was hyperactive and showed an upward and rightward shift in the dose response with more than a 2-fold increase in EC_{50} value of 1497 ± 310 μM (Fig. 3*A*, *panel VI*). The complementary mutation, K270R, showed a similar dose response as WT-T2R4 with an EC_{50} value of 780 ± 180 μM. Representative raw calcium traces for the mock-transfected (pcDNA3.1) cells, WT-T2R4, and all the mutants are shown in Fig. 3*B*.

Proper cell surface expression/localization of a GPCR is normally used as an indicator of correct protein folding. The T2R4 construct used in this study had a FLAG tag at its N terminus, which allowed detection of the receptor on the cell surface by an anti-FLAG antibody, without the need to permeabilize the cells. Using flow cytometry, the cell surface expression of WT-T2R4 and its mutants was analyzed. The mean fluorescence intensity values obtained were normalized to the WT-T2R4, which was taken as 100% (Fig. 3*C*). The majority of the mutants, including A90G, F91A, N173Q, T174S, Y258A, and K270R, showed proper expression on the surface of HEK293T cells, similar to WT-T2R4. The mutants Y155A, N172A, and T174A showed 30–40% increased expression levels compared with that of WT-T2R4. Three mutants A90F, F92A, and K270A, showed up to a 40% decrease in cell surface expression. However, no statistical significance in expression levels between the different mutants and WT-T2R4 was observed (Fig. 3*C*).

To characterize the basal or constitutive activity of the two hyperactive mutants A90F and K270A, agonist-independent IP_3 production was measured. A previously characterized constitutively active mutant (CAM) of T2R4, H214A, was used as a positive control. Both A90F and K270A mutants showed a statistically significant increase in agonist-independent IP_3 production of 480 ± 28 and 520 ± 17 nmol over WT-T2R4 (Fig. 4). The basal IP_3 values produced by unstimulated WT-T2R4 and H214A CAM were 307 ± 36 and 540 ± 33 nmol, respectively (Fig. 4).

Docking of Amino Acid Derivatives to T2R4—After identifying the quinine-binding site on T2R4, this ligand-binding pocket on T2R4 was selected for docking amino acid derivatives. A total of 75 amino acid derivatives from the Sigma commercial database and bitter maskers GABA and OA were docked to T2R4 as described under "Experimental Procedures." The docked compounds were scored using Surflex-Dock, which predicted varying K_d values (Table. 1). Around 19 amino acid derivatives, including GABA and OA, showed predicted binding affinity in the micro- to nanomolar range. The two compounds with the highest predicted binding affinity in the nanomolar range were *N*α-methoxycarbonyl-L-tryptophan methyl ester and BCML. These two compounds, along with GABA and OA, were selected for competition assays to characterize their ligand specificities.

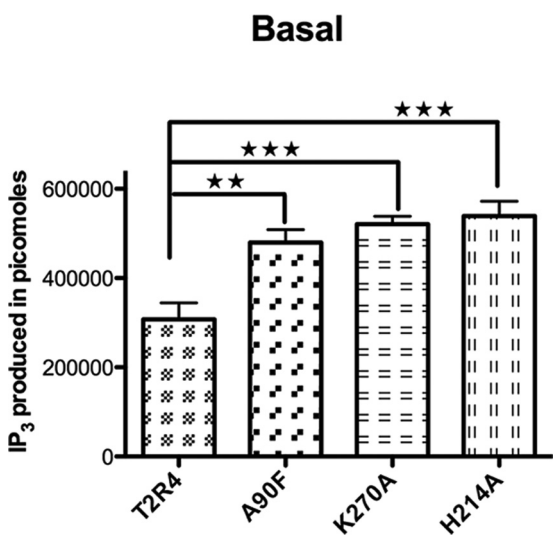

FIGURE 4. **Basal or agonist-independent IP_3 production by T2R4 and mutants A90F and K270A.** Characterization of basal activity was done as described under "Experimental Procedures." H214A, a CAM of T2R4, was used as a positive control. Both A90F and K270A showed statistically significant high basal activity, with K270A showing constitutive activity similar to H214A. Results are from three independent experiments performed in triplicate. One-way analysis of variance was performed followed by Tukey's multiple comparison post hoc tests to check the significance, and $p < 0.05$ was considered significant. *, $p \leq 0.05$; **, $p \leq 0.01$; ***, $p \leq 0.001$.

Functional Characterization of the Potential Bitter Blockers—The ability of the four compounds to activate T2R4 expressed in HEK293T cells was analyzed. However, no activation of T2R4 was observed. Next, competition calcium mobilization assays were pursued. T2R4 was treated with increasing concentrations of each of the four ligands in the presence of 1 mM quinine, and the half-maximum inhibitory concentration (IC_{50}) was analyzed (Fig. 5*A*). Of the four compounds, only GABA and BCML showed antagonist activity, with IC_{50} values of 3.2 ± 0.3 μM and 59 ± 18 nM respectively (Fig. 5*A*). OA and *N*α-methoxycarbonyl-L-tryptophan methyl ester did not inhibit T2R4. Representative raw calcium traces for the mock-transfected (pcDNA3.1) HEK293T cells and WT-T2R4 treated with GABA or BCML in the absence and presence of quinine are shown in Fig. 5*B*.

FIGURE 3. **Characterization of Gα16/44 chimera-mediated signaling of T2R4 and quinine-binding pocket mutants.** *A,* concentration-dependent changes in intracellular [Ca^{2+}] induced by bitter ligand quinine in HEK293T cells transiently expressing the chimeric Gα16/gust44 and WT-T2R4 or mutants. Data were collected from at least three independent experiments carried out in duplicate. Changes in intracellular calcium were measured by using calcium-binding dye Fluo-4 NW, and data were analyzed by GraphPad Prism software, after subtracting the responses of mock-transfected cells. *B,* representative raw calcium traces for the mock-transfected (pcDNA3.1) cells, T2R4, and all the mutants. The time point (20 s) at which the agonist quinine (4 mM) was added to the assay is shown by *arrows*. *C,* cell surface expression of T2R4 and mutants. Cell surface expression studies were carried out by flow cytometry using the anti-FLAG antibody, which binds to the FLAG sequence at the N terminus of the T2R4 and mutant receptors. The mean fluorescence intensities of the mutants were normalized to wild type and expressed in terms of percentage. No statistically significant difference in expression was observed between the T2R4 and the mutants.

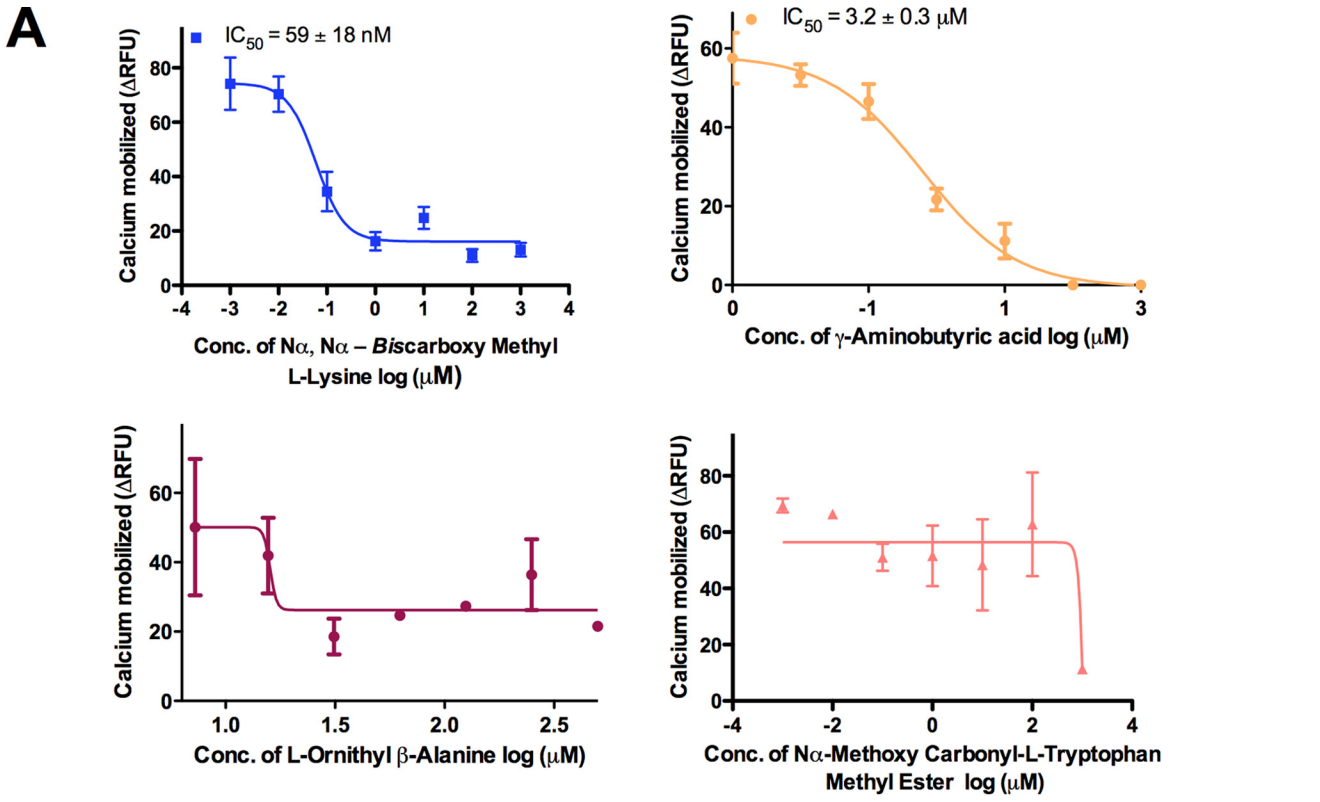
A
IC50 = 59 ± 18 nM
Calcium mobilized (ΔRFU)
Conc. of Nα, Nα – Biscarboxy Methyl L-Lysine log (μM)
IC50 = 3.2 ± 0.3 μM
Conc. of γ-Aminobutyric acid log (μM)
Conc. of L-Ornithyl β-Alanine log (μM)
Conc. of Nα-Methoxy Carbonyl-L-Tryptophan Methyl Ester log (μM)

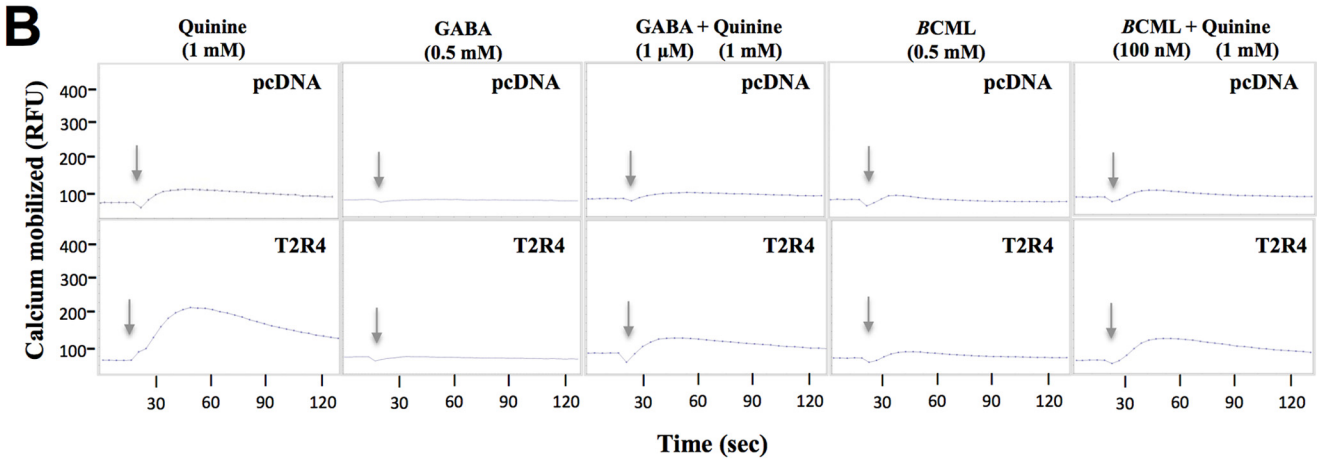
B
Quinine (1 mM)
GABA (0.5 mM)
GABA + Quinine (1 μM) (1 mM)
BCML (0.5 mM)
BCML + Quinine (100 nM) (1 mM)
pcDNA
T2R4
Calcium mobilized (RFU)
Time (sec)

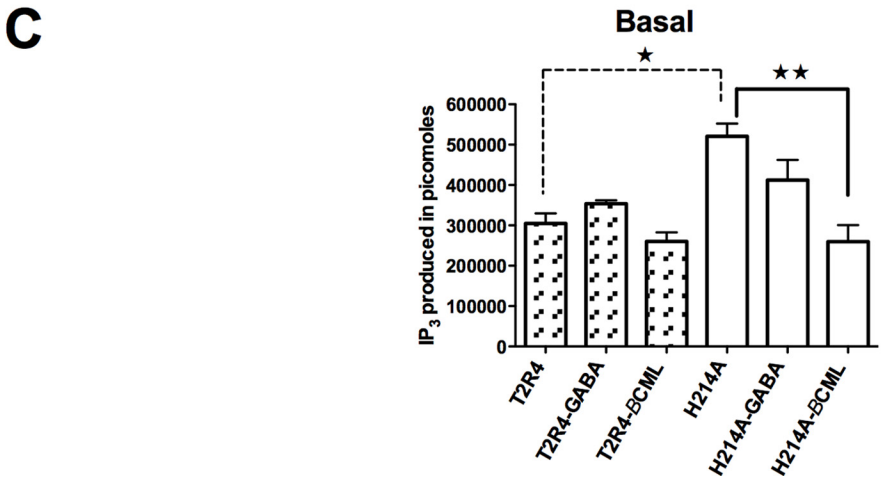
C
Basal
IP3 produced in picomoles
T2R4
T2R4-GABA
T2R4-BCML
H214A
H214A-GABA
H214A-BCML

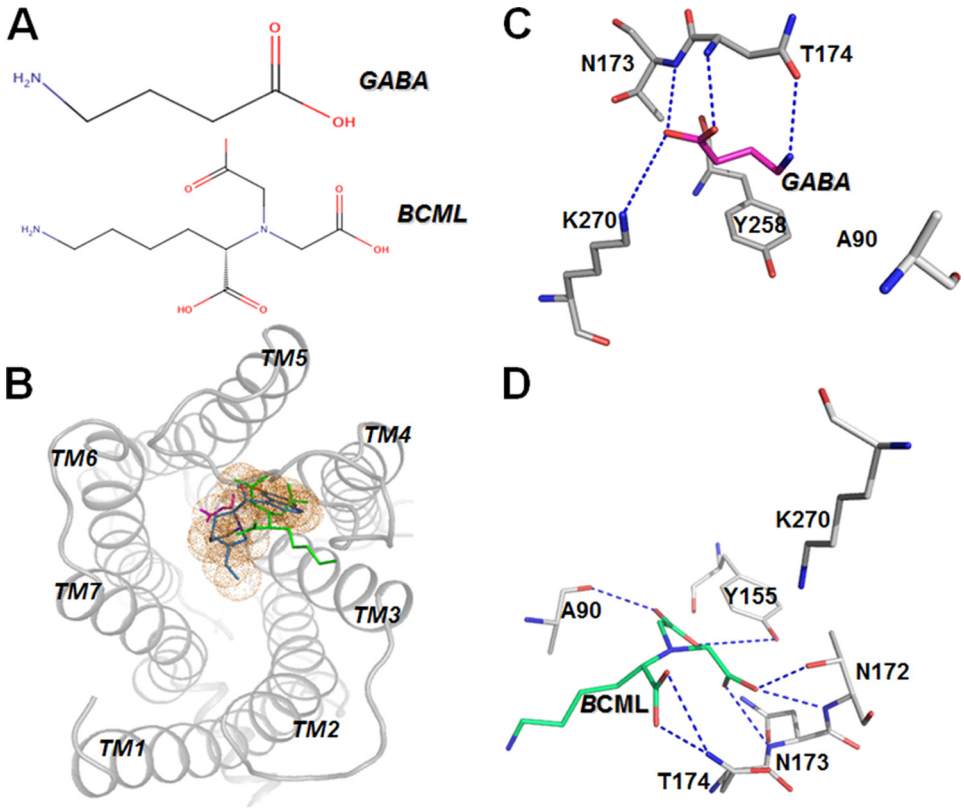

FIGURE 6. **Bitter blockers GABA, BCML, and their binding pocket in T2R4.** *A,* two-dimensional chemical structures of GABA and BCML. GABA is not a typical α-amino acid. BCML is a lysine derivative consisting of three carboxylate functional groups. *B,* agonist, antagonist, and inverse agonist-binding pocket in T2R4. Overlap image of binding pocket of quinine, GABA, and BCML. The compounds bind within the same binding pocket but in different orientations. *C,* T2R4 residues interacting with GABA are represented in *gray* and GABA is represented in *pink*. *D,* residues interacting with BCML. BCML showed the highest number of T2R4 contacts when compared with quinine and GABA. The H-bonds are represented by *blue lines*.

GPCR CAMs can be used as pharmacological tools to classify ligands into neutral antagonists and inverse agonists (26, 27). Neutral antagonists are compounds that do not affect the basal GPCR activity and have zero efficacy, whereas inverse agonists are known to reduce basal GPCR activity and are often defined as having a −1 efficacy. To further characterize the bitter blocking activity of BCML and GABA, the effects of these two T2R4 antagonists on constitutive IP_3 produced by WT-T2R4 and the previously reported H214A CAM were studied. The concentration of GABA and BCML used in these experiments was 3.2 μM and 59 nM, which were their IC_{50} values. No statistically significant effects were observed for GABA and BCML on the basal activity of WT-T2R4 (Fig. 5*C*). Interestingly, 59 nM BCML was able to decrease the basal activity of H214A by 40% (Fig. 5*C*). However, no statistically significant change in basal IP_3 production was observed when WT-T2R4 or H214A were treated with 3.2 μM GABA.

Characterization of T2R4 Residues Involved in Binding to GABA and BCML—Molecular docking studies predicted GABA and BCML to bind T2R4 within the same binding pocket as quinine but in different orientations (Fig. 6, *A* and *B*). Asn-173 and Thr-174 are critical residues on T2R4 that interact with all three ligands, quinine, GABA, and BCML. However, GABA and BCML have their own unique interactions. The ϵ-amino group of Lys-270 is predicted to interact with the O1-carboxyl of GABA (Fig. 6*C*). Residues Ala-90, Tyr-155, and Asn-172 are found interacting with the three carboxyl groups of BCML (Fig. 6*D*). Mutations of amino acids Tyr-155, Asn-172, Asn-173, and Thr-174 could not be used for functional characterization of GABA and BCML binding, as these are either essential or play important roles in quinine binding. Therefore, we tested the role of A90F and K270A in binding to BCML and GABA, as these are also found to be interacting with BCML and GABA, respectively (Fig. 7*A*). Competition calcium mobilization assays

FIGURE 5. **Functional characterization of potential bitter blockers.** *A,* competition calcium mobilization assays. Cells expressing T2R4 were treated with 1 mM quinine and with increasing concentrations (*Conc.*) (logarithmic) of GABA, BCML, OA, or *N*α-methoxycarbonyl-L-tryptophan methyl ester. Changes in intracellular calcium were measured (RFUs), and IC_{50} values were calculated using GraphPad Prism 4.0. Of the four compounds tested, only GABA and BCML inhibited quinine-induced T2R4 activity, with IC_{50} values of 3.2 ± 0.3 μM and 59 ± 18 nM, respectively. *B,* representative raw calcium traces. Mock-transfected (pcDNA3.1) cells and T2R4-expressing cells were treated with GABA or BCML in the absence and presence of quinine. *Arrows* represent the time point (20 s) when the ligands were added to the assays. GABA (0.5 mM) and BCML (0.5 mM) were unable to activate T2R4. However, both the compounds were able to inhibit the quinine-induced T2R4 activity. *C,* effect of T2R4 antagonists on basal intracellular IP_3 production. HEK293T cells transiently expressing the chimeric Gα16/gust44 and WT-T2R4 or H214A CAM were treated with buffer or 3.2 μM GABA or 59 nM BCML (their IC_{50} values), and the IP_3 produced was measured using Hit Hunter IP_3 fluorescence polarization assay kit. BCML has inverse agonist activity and showed statistically significant reduction of the basal activity of H214A by 40%. Data were collected from at least three independent experiments carried out in triplicate. Values are plotted as mean ± S.E. *, $p \leq 0.05$; **, $p \leq 0.01$.

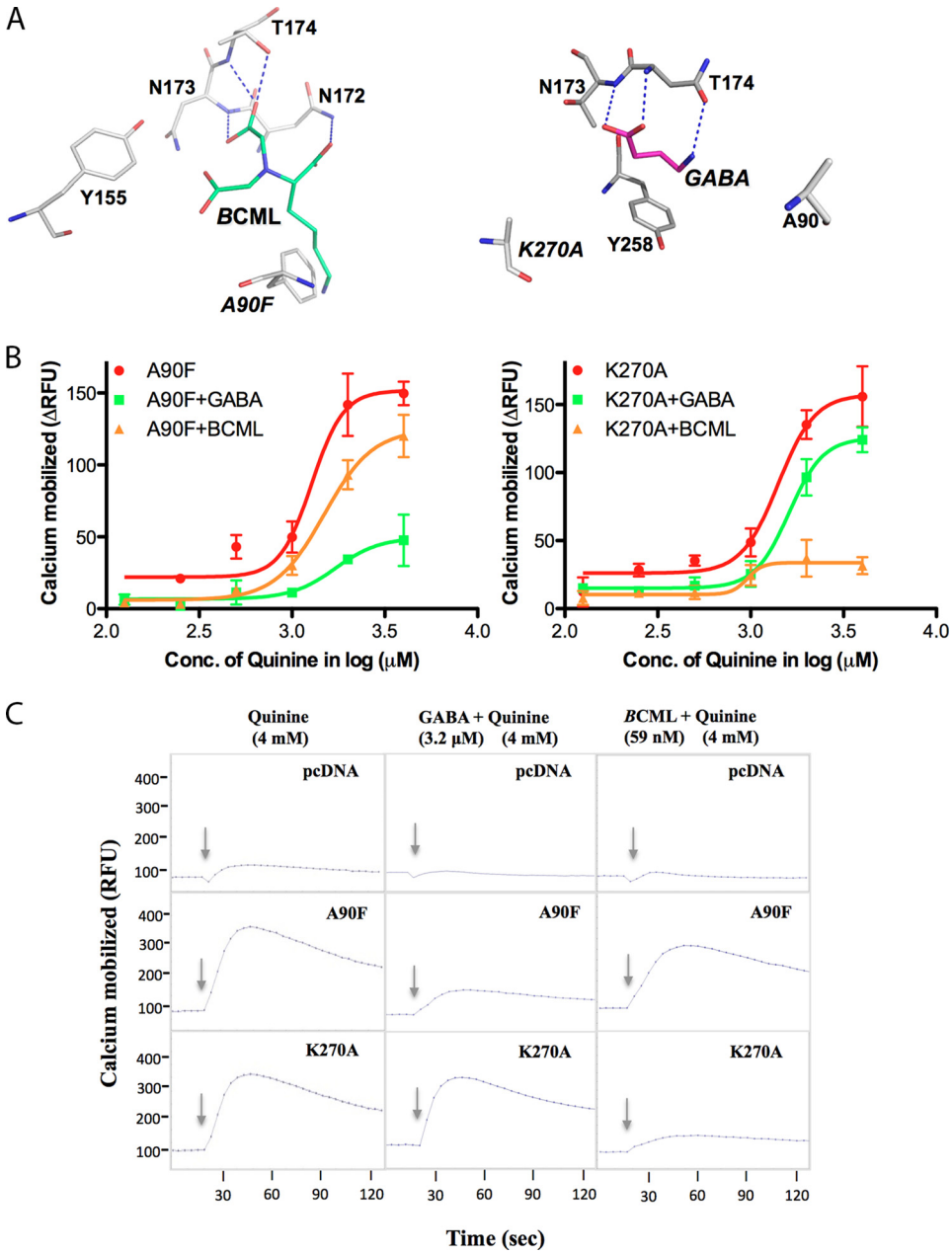

FIGURE 7. **Functional characterization of T2R4 residues important for GABA and BCML binding.** *A,* A90F and K270A molecular models were docked with BCML and GABA. In the WT-T2R4 model, it was observed that A90F is important for BCML binding, and K270A is important for GABA binding. In the mutant models, these interactions were completely lost. *B,* competition dose-response assays of A90F and K270A mutants. Cells expressing A90F and K270A mutants were stimulated with different concentrations of quinine (0.06–4 mM), in the presence and absence of IC_{50} concentrations of BCML (59 nM) or GABA (3.2 μM). Changes in intracellular calcium mobilized were measured (Δ*RFUs*). All the experiments were repeated three times in triplicate. Ala-90 and Lys-270 are important for BCML and GABA binding, respectively. *C,* representative raw calcium traces for the mock-transfected (*pcDNA3.1*)-, A90F-, and K270A-expressing cells. The cells were treated with a single saturating concentration of quinine (4 mM) and with IC_{50} value concentrations of GABA (3.2 μM) or BCML (59 nM) in the presence of quinine. *Arrows* represent the time point (20 s) at which the ligands were added to the assays.

showed that GABA (3.2 μM) does not suppress the quinine concentration-dependent activity of K270A (Fig. 7*B*). The EC_{50} values of K270A and K270A + GABA are within the range (1497 ± 310 μM *versus* 1609 ± 120 μM), but BCML (59 nM) completely inhibited the agonist-dependent activity of K270A (Fig. 7*B*). Interestingly, in the case of A90F, it is not BCML but GABA that inhibits agonist-dependent activity of A90F (Fig. 7*B*). The EC_{50} values of A90F and A90F + BCML are very similar (1280 ± 190 μM *versus* 1480 ± 150 μM). Representative raw calcium traces for the mock-transfected (pcDNA3.1) cells, A90F, and K270A treated with a single saturating concentration of quinine (4 mM), and GABA or BCML in the presence of quinine are shown in Fig. 7*C*. These results confirm the interactions of T2R4 residues Ala-90 with BCML and Lys-270 with GABA.

DISCUSSION

Within the GPCR superfamily, there is remarkable diversity in the location, shape, and features of the ligand-binding pocket. For example, in class A GPCRs, the ligand binds within

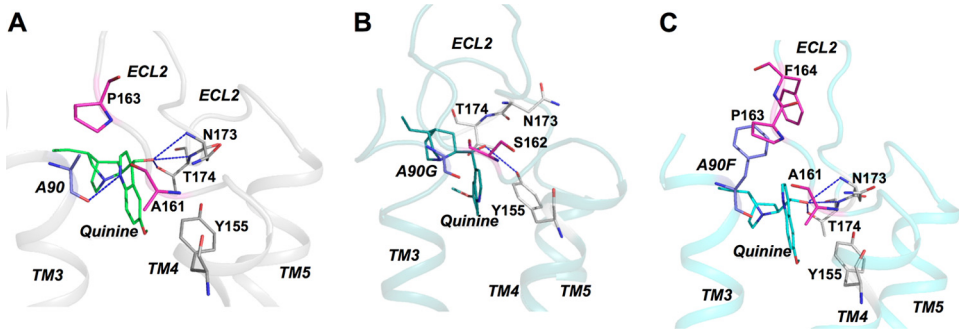

FIGURE 8. **Molecular model analysis of the ligand-binding pocket of T2R4, A90G, and A90F mutants.** T2R4, A90G, and A90F molecular models were docked with quinine using Surflex-Dock program, and the docked complexes were analyzed using PyMOL. *A,* in T2R4 docked with quinine, Ala-90 of TM3 is packed between Ala-161 and Pro-163, which are present at the interface of TM4-ECL2. In this model, quinine is interacting with the backbone of Ala-90 and Asn-173 and Thr-174 of ECL2. *B,* in A90G model docked with quinine, Gly-90 was packed against Ser-162, and the H-bond interactions between quinine and the backbone of Ala-90, Asn-173, and Thr-174 were lost, and a new H-bond was observed between quinine and Tyr-155. *C,* in A90F model docked with quinine, Phe-90 is packed against Ala-161, Pro-163, and Phe-164. The H-bonds between quinine and Asn-173 and Thr-174 were intact. This explains the ability of the T2R4 Phe-90 mutant to get activated by quinine.

a pocket that is lined by amino acids from the extracellular loops and extracellular side of TM regions (28–30). However, in class C GPCRs, including metabotropic glutamate receptors (mGluRs), sweet and umami taste receptors (T1Rs), there are multiple ligand-binding sites, including an orthosteric site in the N-terminal domain also referred to as the Venus flytrap domain. The recent 2.8 Å structure of mGlu1 shows that an allosteric modulator site partially overlaps the orthosteric binding site seen in class A GPCRs (31). Similar to other GPCRs, T2Rs have the ability to bind to ligands of diverse chemical properties, shapes, and sizes. However, unlike T1Rs, T2Rs are not reported to have an allosteric binding site but similar to most class A GPCRs possess only an orthosteric site. Because some T2R ligands are small, they were hypothesized to bind deep within the TM core. However, there is growing evidence suggesting a role for extracellular loops in the ligand binding in T2Rs. Swapping of ECL1 between T2R43 and T2R44 showed defective agonist binding when the T2R43 chimera was stimulated with its agonist *n*-isopropyl-2-methyl-5-nitrobenzenesulfonamide (14). Similarly, with T2R46 the ECL2 mutant N150K displayed reduced agonist binding (14). In most of the T2Rs, TM3 plays a crucial role in ligand binding (13, 15, 32–35). In the first part of this structure-function study, the quinine-binding pocket of the moderately tuned T2R4 was elucidated.

T2R4 Mutants and Quinine Binding—The molecular model of the T2R4-quinine complex shows that the backbone of Ala-90 is forming an H-bond with the *N*-group of the quinolone ring of quinine. Interestingly, the A90G mutant was inactive, whereas A90F is constitutively active and showed hyperactivity upon stimulation with quinine (Figs. 3*A* and 4). We also observed a right shift in the dose-response curve of A90F with a 2-fold increase in the EC_{50} value when compared with WT-T2R4. To interpret these results in detail, molecular models of A90G and A90F bound to quinine were constructed and analyzed (Fig. 8). In T2R4-WT, Ala-90 of TM3 is packed between Ala-161 and Pro-163, which are present at the interface of TM4-ECL2 (Fig. 8*A*). In this model, quinine is interacting with backbone of Ala-90 and side chains of ECL2 residues Asn-173 and Thr-174. Mutational studies of Asn-173 and Thr-174 confirmed that these residues are crucial for quinine binding. In the T2R4-A90G model, the H-bond interactions between quinine and Gly-90 and between Asn-173 and Thr-174 were completely lost, and a new H-bond was observed between quinine and Tyr-155 (Fig. 8*B*). ECL2 also attained a more open confirmation when compared with WT-T2R4. Similar results were observed in a class A GPCR, thromboxane A_2 receptor, and when Gly-164 of TM4 was mutated to valine, the crucial interactions between the antagonist and ECL2 residue Ser-191 were lost (36). In theT2R4-A90F model, the H-bond network between quinine and the two ECL2 residues, Asn-173 and Thr-174, were intact (Fig. 8*C*). This explains the ability of Phe-90 mutant to be activated by quinine. However, the presence of the bulky phenylalanine (A90F) caused a steric clash with Pro-163 and Phe-164 at the extracellular side of TM4, which resulted in the movement of TM3 away from TM4. This movement of TM3 might have resulted in the high basal activity of A90F (Fig. 4). It is well established that TM3 plays a crucial role in GPCR activation and is a hot spot for CAMs in a number of GPCRs. The F91A mutant was not activated by quinine in a concentration-dependent manner (Fig. 3), and this may be due to the presence of F91A next to the important Ala-90, thereby indirectly influencing quinine binding through modulation of Ala-90 residue. The only residue from TM4 involved in quinine binding was Tyr-155. Molecular modeling suggested π-π stacking interactions between the quinolone ring of quinine and the aromatic ring of Tyr-155 (Fig. 2). In the Y155A mutant, these interactions were lost and resulted in the loss of function (Fig. 3*A*).

Based on molecular modeling, two residues in T2R4 ECL2, Asn-173 and Thr-174, were involved in H-bond with the hydroxyl group of quinine. Asn-173 was mutated to alanine (N173A) and to a functionally similar residue glutamine (N173Q), and no functional response was observed for both mutants. It suggests that Asn-173 is essential for binding to quinine and both length of the side chain, and H-bond capability at position 173 is crucial. Similar results were observed with Thr-174 mutations. The T174A mutant resulted in complete loss of function, whereas the complementary substitution T174S was able to signal albeit at reduced levels with a 2.5-fold increase in EC_{50} value compared with WT-T2R4. It suggests that the ability of the residue at position 174 to H-bond is important. In T2R4-ECL3 there are two residues predicted to

be involved in quinine binding, and these are present at either end of ECL3. Tyr-258 is present at the beginning of ECL3, and Lys-270 is present at the end, in the ECL3-TM7 intersection. Based on molecular modeling, the quinoline ring of quinine is stacked between Tyr-155 and Tyr-258 (Fig. 2*C*). The Y258A mutant showed complete loss of quinine-induced calcium mobilization (Fig. 3*A*). This result validates the model predicting that Tyr-258 along with Tyr-155 play an essential role in the interaction with the quinoline ring of quinine. Another residue present within the 4-Å region of the quinine-binding pocket in T2R4 was Lys-270. In our T2R4-quinine model, Lys-270 did not make any direct contact with quinine (Fig. 2*C*). Interestingly, the K270A mutant showed hyperactivity (Fig. 3*A*), as well as constitutive activity (Fig. 4). The conservative substitution K270R displayed WT-T2R4 characteristics, implying that a positively charged residue is important at position 270. Unfortunately, our models could not predict a direct role for Lys-270 in quinine binding, and a number of factors could be responsible. It is well known that the conformations of the loops regions in GPCRs are hard to predict, and also the role of structural water molecules in ligand binding was not considered in our models.

Bitter Blockers—The 25 human T2Rs are activated by more than 100 natural and synthetic bitter ligands (16). Strikingly, only five known antagonists are published, these are GIV3727, 3β-hydroxypelenolide, 3β-hydroxydihydrocostunolide, probenecid, and 6-methoxyflavanones (17–20). Compound C from Senomyx Inc. was also reported to act as a bitter blocker. Interestingly, none of these blockers can block all the 25 T2Rs and some of them act as agonists on other T2Rs. For example, GIV3727 acts as an agonist for T2R14, although the Senomyx compound C acts as an agonist for T2R4. Although most of these bitter blockers act as competitive inhibitors, probenecid was reported to act as an allosteric inhibitor on T2R16 (20). Given the ligand diversity of T2Rs, it is highly unlikely that a universal blocker, which can target all 25 human T2Rs, can be developed. Therefore, it is imperative that blockers with high selectivity and efficacy be developed that can target specific T2Rs. A mixture of these blockers can be used to block all the 25 T2Rs if needed.

Based on our analysis of the T2R4 ligand-binding pocket and taking into consideration the published information on the bitter masking abilities of GABA and OA, we pursued a limited virtual ligand screening of the amino acid derivatives (Table 1). Our competition assays show that GABA and BCML act as bitter blockers with IC_{50} values of 3.2 $\pm$ 0.3 μM and 59 $\pm$ 18 nM respectively (Fig. 5*A*). To further elucidate this antagonist activity, we used our unique pharmacological bitter ligand screening method that involves the use of T2R-CAMs to detect whether a given compound is an agonist, antagonist, or inverse agonist for a given T2R (22). Interestingly, pharmacological characterization led to the identification of BCML as an inverse agonist, as it was able to significantly decrease the activity of a T2R4-CAM, H214A (Fig. 5*A*). Molecular docking studies suggest these two blockers share the same ligand-binding pocket as the agonist quinine in T2R4. This was further confirmed by analysis of the site-directed mutants, A90F and K270A, that show that Lys-270 is involved in interactions with GABA, whereas Ala-90 interacts with BCML.

TABLE 1

Amino acid derivatives predicted to bind to T2R4

Amino acid derivatives (commercially available in the Sigma catalogue) were docked with T2R4 using Surflex-Dock program of SYBYL-X 1.3 suite. The binding affinities of protein-ligand complexes were obtained as the total Surflex-Dock score expressed as $-\log(K_d)$. The top two ligands (high affinity) from the table (highlighted in bold) were selected for functional screening using calcium imaging.

Compound name	Predicted binding affinity ($-\log K_d$)	Predicted K_d values
		μM
Nα-Methoxycarbonyl-L-tryptophan methyl ester	**8.47**	**0.0012**
Nα,Nα-Bis(carboxymethyl)-L-lysine	**8.92**	**0.0033**
Benzyloxycarbonyl-Leu-ONp	8.05	0.0090
D-Tryptophan benzyl ester	8.29	0.0051
$N_{(im)}$-Trityl-L-histidine-propylamide	7.44	0.036
N,N-Dibenzyl-L-serine methyl ester	7.33	0.046
L-Aspartic acid β-benzyl ester	7.23	0.059
N-Benzyl-D-proline ethyl ester	7.07	0.085
L-Tyrosine *tert*-butyl ester	7.05	0.089
N-Tritylglycine	6.67	0.213
β-Asp-Phe methyl ester	6.62	0.237
N^{ε}-Trifluoroacetyl-L-lysine	6.53	0.295
$N_{(im)}$-Trityl-L-histidine	6.50	0.316
L-Glutamic acid γ-ethyl ester	6.46	0.346
N,N′-Dibenzoyl-L-cystine	6.36	0.436
N-Benzoyl-L-leucine	6.22	0.603
O-Benzyl-L-threonine	6.00	1.00
H-D-Lys(Alloc)-OH	6.17	0.70
Methyl l-β-aspartyl-L-phenylalaninate	6.12	0.75
4-Aminobenzoylglutamic acid	5.74	1.8
D-Cystine	5.50	3.12
H-Lys(Alloc)-OH	5.30	5.01
L-Tyrosine hydrazide	5.26	5.49
1-Methyl-D-tryptophan	5.18	6.60
H-Arg(MTR)-OH	5.09	8.12
O-tert-Butyl-L-serine	5.02	9.54
3-(2-Naphthyl)-D-alanine	5.01	9.77
O-Benzyl-D-serine	4.98	10.47
N,N-Dibenzyl-L-serine methyl ester	4.78	16.59
Poly-γ-benzyl-L-glutamate	4.56	27.54
H-Lys(Tfa)-OH	4.47	33.88
Poly-β-benzyl-aspartate	4.37	42.65
N-phthaloylglutamic acid	4.30	50.11
N-Benzyl-D-proline ethyl ester	4.18	66.06
α-Ethylglutamic acid	4.11	77.62
O-tert-Butyl-L-threonine	4.10	79.43
S-(*tert*-Butylthio)-L-cysteine	4.04	91.2
N-Carbobenzyloxyalanine	4.00	100.00
N-Acetylglutamic acid	3.96	109.64
1-Methylhistidine	3.83	147.91
S-Phenyl-*N*-acetylcysteine	3.78	165.95
L-Aspartic acid 4-*tert*-butyl ester	3.68	208.92
N-Acetylmethionine	3.67	213.79
O-Methyl-L-tyrosine	3.57	269.15
N-Acetyl-L-phenylalanine	3.41	389.04
L-Methionine sulfoxide	3.35	446.68
L-Methionine sulfone	3.23	588.84
Ethylaceturate	3.07	851.38
O-tert-Butyl-L-tyrosine	3.06	870.96
H-His(Trt)-OH	2.95	1122.01
N-Benzoyl-L-threonine methyl ester	2.83	1479.1
Acetyl-leucine	2.83	1479.1
tert-Butyl (2-(methoxy(methyl)amino)-2-oxoethyl)carbamate	2.76	1737.8
N-Phthalylglycine	2.51	3090.29
N-Formylglycine	2.48	3311.31
Hippuric acid	2.23	5888.43

GABA and BCML as T2R4 Blockers—The discovery of GABA and BCML as antagonists and inverse agonists of T2R4 is very interesting. GABA is the primary inhibitory neurotransmitter in the mammalian central nervous system and acts by binding to membrane proteins, including family C GPCRs. GABA is also synthesized in the taste buds and acts as an inhibitory transmitter and suppresses other transmitter (ATP) secretions

from type II taste receptor cells during taste stimulation (37, 38). The antagonist activity of GABA on T2R4 reported in this study makes it the first endogenous bitter blocker. Furthermore, it provides a new action of GABA directly on T2Rs *per se*, in addition to its known action on taste receptor-containing cells. Outside the central nervous system, GABA is also found in airway epithelium, stomach, lungs, kidney, blood cells, pancreas, and testis (39). Recent studies showed the expression of T2R4 in human leukocytes, airways, trachea, colon, gut, and heart. It is possible that GABA might be playing a key role in regulating the function of T2R4 in some of these tissues or organs. BCML is a derivative of the advanced glycation end (AGE) product carboxymethyl-lysine. We also tested carboxymethyl-lysine for its antagonist activity on T2R4, but no reduction in quinine-dependent activity was observed (data not shown). In our study, we did not test all the AGEs and therefore cannot rule out the possibility that other AGEs may block or activate T2Rs. More studies are required to identify the role of AGEs in activating or blocking T2Rs in physiological conditions. The only published antagonist for T2R4 was GIV3727; however, it was reported to cause only 50% inhibition of T2R4 (17). The IC_{50} value of BCML is around 59 nM, making it the first bitter blocker to have potency in the lower nanomolar range. Strikingly, BCML shows inverse agonist activity. The antagonist activity of GABA and BCML on the remaining 24 T2Rs remains to be analyzed. Most of the drugs used in various disease conditions are bitter and have off-target effects. Recent studies have shown that T2Rs play a key role in these off-target effects as these drugs can activate T2Rs (40). Highly potent bitter blockers can be used to reduce the side effects of bitter drugs. The molecular events in the signal transduction of T2Rs in various cell types are not understood. These blockers can be used to understand the expression profile and signaling pathways in different cell types. In addition, the bitter blockers can be used in the elimination of bitter taste in dietary foods that provide health benefits.

In conclusion, this study led to the characterization of the ligand-binding pocket of T2R4 and identified residues essential for binding of the bitter agonist quinine. Two novel bitter blockers, GABA and BCML, were identified and characterized. Interestingly, both the agonists and blockers share the same orthosteric site in T2R4. Considering the wide distribution of T2Rs in extraoral tissues, the endogenous nature of GABA and the low nanomolar affinity of BCML for T2R4 give them immense potential for use in physiological and structural studies.

REFERENCES

1. Hoon, M. A., Adler, E., Lindemeier, J., Battey, J. F., Ryba, N. J., and Zuker, C. S. (1999) Putative mammalian taste receptors: a class of taste-specific GPCRs with distinct topographic selectivity. *Cell* **96,** 541–551
2. Chandrashekar, J., Mueller, K. L., Hoon, M. A., Adler, E., Feng, L., Guo, W., Zuker, C. S., and Ryba, N. J. (2000) T2Rs function as bitter taste receptors. *Cell* **100,** 703–711
3. Finger, T. E., Böttger, B., Hansen, A., Anderson, K. T., Alimohammadi, H., and Silver, W. L. (2003) Solitary chemoreceptor cells in the nasal cavity serve as sentinels of respiration. *Proc. Natl. Acad. Sci. U.S.A.* **100,** 8981–8986
4. Chen, X., Gabitto, M., Peng, Y., Ryba, N. J., and Zuker, C. S. (2011) A gustotopic map of taste qualities in the mammalian brain. *Science* **333,** 1262–1266
5. Singh, N., Vrontakis, M., Parkinson, F., and Chelikani, P. (2011) Functional bitter taste receptors are expressed in brain cells. *Biochem. Biophys. Res. Commun.* **406,** 146–151
6. Wu, S. V., Rozengurt, N., Yang, M., Young, S. H., Sinnett-Smith, J., and Rozengurt, E. (2002) Expression of bitter taste receptors of the T2R family in the gastrointestinal tract and enteroendocrine STC-1 cells. *Proc. Natl. Acad. Sci. U.S.A.* **99,** 2392–2397
7. Wu, S. V., Chen, M. C., and Rozengurt, E. (2005) Genomic organization, expression, and function of bitter taste receptors (T2R) in mouse and rat. *Physiol. Genomics* **22,** 139–149
8. Deshpande, D. A., Wang, W. C., McIlmoyle, E. L., Robinett, K. S., Schillinger, R. M., An, S. S., Sham, J. S., and Liggett, S. B. (2010) Bitter taste receptors on airway smooth muscle bronchodilate by localized calcium signaling and reverse obstruction. *Nat. Med.* **16,** 1299–1304
9. Shah, A. S., Ben-Shahar, Y., Moninger, T. O., Kline, J. N., and Welsh, M. J. (2009) Motile cilia of human airway epithelia are chemosensory. *Science* **325,** 1131–1134
10. Singh, N., Pydi, S. P., Upadhyaya, J., and Chelikani, P. (2011) Structural basis of activation of bitter taste receptor T2R1 and comparison with class A G-protein-coupled receptors (GPCRs). *J. Biol. Chem.* **286,** 36032–36041
11. Born, S., Levit, A., Niv, M. Y., Meyerhof, W., and Behrens, M. (2013) The human bitter taste receptor TAS2R10 is tailored to accommodate numerous diverse ligands. *J. Neurosci.* **33,** 201–213
12. Levit, A., Nowak, S., Peters, M., Wiener, A., Meyerhof, W., Behrens, M., and Niv, M. Y. (2014) The bitter pill: clinical drugs that activate the human bitter taste receptor TAS2R14. *FASEB J.* **28,** 1181–1197
13. Sakurai, T., Misaka, T., Ishiguro, M., Masuda, K., Sugawara, T., Ito, K., Kobayashi, T., Matsuo, S., Ishimaru, Y., Asakura, T., and Abe, K. (2010) Characterization of the β-D-glucopyranoside binding site of the human bitter taste receptor hTAS2R16. *J. Biol. Chem.* **285,** 28373–28378
14. Pronin, A. N., Tang, H., Connor, J., and Keung, W. (2004) Identification of ligands for two human bitter T2R receptors. *Chem. Senses* **29,** 583–593
15. Brockhoff, A., Behrens, M., Niv, M. Y., and Meyerhof, W. (2010) Structural requirements of bitter taste receptor activation. *Proc. Natl. Acad. Sci. U.S.A.* **107,** 11110–11115
16. Meyerhof, W., Batram, C., Kuhn, C., Brockhoff, A., Chudoba, E., Bufe, B., Appendino, G., and Behrens, M. (2010) The molecular receptive ranges of human TAS2R bitter taste receptors. *Chem. Senses* **35,** 157–170
17. Slack, J. P., Brockhoff, A., Batram, C., Menzel, S., Sonnabend, C., Born, S., Galindo, M. M., Kohl, S., Thalmann, S., Ostopovici-Halip, L., Simons, C. T., Ungureanu, I., Duineveld, K., Bologa, C. G., Behrens, M., Furrer, S., Oprea, T. I., and Meyerhof, W. (2010) Modulation of bitter taste perception by a small molecule hTAS2R antagonist. *Curr. Biol.* **20,** 1104–1109
18. Roland, W. S., Gouka, R. J., Gruppen, H., Driesse, M., van Buren, L., Smit, G., and Vincken, J. P. (2014) 6-Methoxyflavanones as bitter taste receptor blockers for hTAS2R39. *PLoS One* **9,** e94451
19. Brockhoff, A., Behrens, M., Roudnitzky, N., Appendino, G., Avonto, C., and Meyerhof, W. (2011) Receptor agonism and antagonism of dietary bitter compounds. *J. Neurosci.* **31,** 14775–14782
20. Greene, T. A., Alarcon, S., Thomas, A., Berdougo, E., Doranz, B. J., Breslin, P. A., and Rucker, J. B. (2011) Probenecid inhibits the human bitter taste receptor TAS2R16 and suppresses bitter perception of salicin. *PLoS One* **6,** e20123
21. Ley, J. P. (2008) Masking bitter taste by molecules. *Chemosensory Perception* **1,** 58–77
22. Pydi, S. P., Bhullar, R. P., and Chelikani, P. (2014) Constitutive activity of bitter taste receptors. *Adv Pharmacol.* **70,** 303–326
23. Pydi, S. P., Singh, N., Upadhyaya, J., Bhullar, R. P., and Chelikani, P. (2014) The third intracellular loop plays a critical role in bitter taste receptor activation. *Biochim. Biophys. Acta* **1838,** 231–236
24. Pydi, S. P., Bhullar, R. P., and Chelikani, P. (2012) Constitutively active mutant gives novel insights into the mechanism of bitter taste receptor activation. *J. Neurochem.* **122,** 537–544
25. Pydi, S. P., Chakraborty, R., Bhullar, R. P., and Chelikani, P. (2013) Role of rhodopsin N terminus in structure and function of rhodopsin-bitter taste receptor chimeras. *Biochem. Biophys. Res. Commun.* **430,** 179–182
26. Bylund, D. B., and Toews, M. L. (2014) Quantitative *versus* qualitative data:

the numerical dimensions of drug action. *Biochem. Pharmacol.* **87,** 25–39
27. Chakraborty, R., Bhullar, R. P., Dakshinamurti, S., Hwa, J., and Chelikani, P. (2014) Inverse agonism of SQ 29,548 and Ramatroban on thromboxane A2 receptor. *PLoS ONE* **9,** e85937
28. Katritch, V., Cherezov, V., and Stevens, R. C. (2012) Diversity and modularity of G protein-coupled receptor structures. *Trends Pharmacol. Sci.* **33,** 17–27
29. Cherezov, V., Rosenbaum, D. M., Hanson, M. A., Rasmussen, S. G., Thian, F. S., Kobilka, T. S., Choi, H. J., Kuhn, P., Weis, W. I., Kobilka, B. K., and Stevens, R. C. (2007) High-resolution crystal structure of an engineered human beta2-adrenergic G protein-coupled receptor. *Science* **318,** 1258–1265
30. Kruse, A. C., Hu, J., Kobilka, B. K., and Wess, J. (2014) Muscarinic acetylcholine receptor x-ray structures: potential implications for drug development. *Curr. Opin. Pharmacol.* **16,** 24–30
31. Wu, H., Wang, C., Gregory, K. J., Han, G. W., Cho, H. P., Xia, Y., Niswender, C. M., Katritch, V., Meiler, J., Cherezov, V., Conn, P. J., and Stevens, R. C. (2014) Structure of a class C GPCR metabotropic glutamate receptor 1 bound to an allosteric modulator. *Science* **344,** 58–64
32. Upadhyaya, J., Pydi, S. P., Singh, N., Aluko, R. E., and Chelikani, P. (2010) Bitter taste receptor T2R1 is activated by dipeptides and tripeptides. *Biochem. Biophys. Res. Commun.* **398,** 331–335
33. Behrens, M., and Meyerhof, W. (2013) Bitter taste receptor research comes of age: from characterization to modulation of TAS2Rs. *Semin. Cell Dev. Biol.* **24,** 215–221
34. Biarnés, X., Marchiori, A., Giorgetti, A., Lanzara, C., Gasparini, P., Carloni, P., Born, S., Brockhoff, A., Behrens, M., and Meyerhof, W. (2010) Insights into the binding of phenylthiocarbamide (PTC) agonist to its target human TAS2R38 bitter receptor. *PLoS One* **5,** e12394
35. Sakurai, T., Misaka, T., Ueno, Y., Ishiguro, M., Matsuo, S., Ishimaru, Y., Asakura, T., and Abe, K. (2010) The human bitter taste receptor, hTAS2R16, discriminates slight differences in the configuration of disaccharides. *Biochem. Biophys. Res. Commun.* **402,** 595–601
36. Chakraborty, R., Pydi, S. P., Gleim, S., Dakshinamurti, S., Hwa, J., and Chelikani, P. (2012) Site-directed mutations and the polymorphic variant Ala160Thr in the human thromboxane receptor uncover a structural role for transmembrane helix 4. *PLoS One* **7,** e29996
37. Cao, Y., Zhao, F. L., Kolli, T., Hivley, R., and Herness, S. (2009) GABA expression in the mammalian taste bud functions as a route of inhibitory cell-to-cell communication. *Proc. Natl. Acad. Sci. U.S.A.* **106,** 4006–4011
38. Dvoryanchikov, G., Huang, Y. A., Barro-Soria, R., Chaudhari, N., and Roper, S. D. (2011) GABA, its receptors, and GABAergic inhibition in mouse taste buds. *J. Neurosci.* **31,** 5782–5791
39. Erdö, S. L., and Wolff, J. R. (1990) γ-Aminobutyric acid outside the mammalian brain. *J. Neurochem.* **54,** 363–372
40. Clark, A. A., Liggett, S. B., and Munger, S. D. (2012) Extraoral bitter taste receptors as mediators of off-target drug effects. *FASEB J.* **26,** 4827–4831